Remote Sensing Applications: Society and Environment 35 (2024) 101210

Contents lists available at ScienceDirect

Remote Sensing Applications: Society and Environment

journal homepage: www.elsevier.com/locate/rsase

Is the change deforestation? Using time-series analysis of satellite data to disentangle deforestation from other forest degradation causes

Ignacio Fuentes [a,b,*], Javier Lopatin [c,d], Mauricio Galleguillos [c], Andrés Ceballos-Comisso [c], Susana Eyheramendy [c], Rodrigo Carrasco [e]

[a] *Facultad de Medicina Veterinaria y Agronomía, Universidad de Las Américas, Sede Providencia, Santiago, Chile*
[b] *Núcleo en Ciencias Ambientales y Alimentarias (NCAA), Universidad de las Américas, Santiago, Chile*
[c] *Facultad de Ingeniería y Ciencias, Universidad Adolfo Ibáñez, Santiago, Chile*
[d] *Fundación Data Observatory, Santiago, Chile*
[e] *Institute of Mathematical and Computational Engineering & School of Engineering, Pontificia Universidad Católica de Chile, Santiago, Chile*

ARTICLE INFO

Keywords:
Deforestation
Remote sensing
Temporal segmentation
Structural breaks

ABSTRACT

Protecting natural ecosystems requires monitoring approaches that work as early warning systems to avoid degradation and protect biodiversity. However, separating forest disturbance causes in change-detection pipelines is challenging due to the complex interplay of multiple drivers affecting vegetation. This study aims to detect deforestation in highly heterogeneous ecosystems. We used Landsat NDVI time-series data for testing three unsupervised change detection methods: (1) the non-parametric phenological anomaly detection (npphen), (2) the continuous change detection and classification (CCDC), and (3) the pruned exact linear time (PELT) algorithms. We used visual interpretation of Google Earth Pro high-resolution data (<10 m) to depict deforestation, and natural-induced changes, like forest browning and fires, evaluating the performance of the unsupervised methods. Additionally, a Random Forest model trained with the outputs from detection algorithms together with elevation and radar vegetation index data were utilised to depict deforestation in a second step. While PELT slightly outperformed other methods for tracking general vegetation changes, with overall accuracies (OA) ranging from 0.78 to 0.99, depending on the vegetation type, it also showed the slowest deforestation tracking response. CCDC presented the fastest response and an OA between 0.78 and 0.95. Additionally, we observed a mean OA of only 0.47 when separating deforestation from other changes using only the unsupervised models. On the other hand, deforestation was accurately detected (OA = 0.93; kappa = 0.83) when using CCDC outputs within a secondary supervised classification, agreeing with selected citizen-based complaints from the Environmental Superintendence. The relatively fast response in deforestation tracking using CCDC makes it a viable alternative for near real-time monitoring. Commonly used unsupervised detection methods may be coupled with supervised techniques to depict vegetation change sources robustly. This application constitutes a step forward for managing and monitoring vegetation areas in highly complex and dynamic landscapes, like Mediterranean ecosystems.

* Corresponding author at: Facultad de Medicina Veterinaria y Agronomía, Universidad de Las Américas, Sede Providencia, Santiago, Chile.
E-mail address: ifuentes@udla.cl (I. Fuentes).

https://doi.org/10.1016/j.rsase.2024.101210
Received 6 February 2024; Received in revised form 20 March 2024; Accepted 24 April 2024
Available online 30 April 2024
2352-9385/

1. Introduction

Monitoring forest ecosystems is crucial for addressing global change and improving environmental monitoring to mitigate ecosystem impairment (Parr et al., 2003; Kofinas, 2009; Bakker and Ritts, 2018; Dong et al., 2019). Forests are essential components of the biosphere functioning and deliver relevant ecosystem services, including the provision and regulation of water and carbon (Bengtsson et al., 2000; Nadrowski et al., 2010; Masek et al., 2015; Song et al., 2016; Löf et al., 2019), nutrient cycling (Attiwill and Adams, 1993; Longo et al., 2020), air purification (Song et al., 2016; Bottalico et al., 2017), biodiversity maintenance (de Oliveira Roque et al., 2018), climate regulation (Figueroa and Pasten, 2015), and recreation (Sánchez et al., 2021).

Deforestation, a global environmental issue, is causing the reduction and shrinking of forest areas (Ribeiro et al., 2011; Hansen et al., 2013; Keenan et al., 2015; Payn et al., 2015; Leblois et al., 2017; Ritchie and Roser, 2021). Deforestation implies changes from forests to other land use classes, which humans or other agents can cause (FAO, 2022). Deforestation is driven by various factors, with urban expansion and agricultural activities being prominent drivers in many regions (DeFries et al., 2010; Leblois et al., 2017). The conversion of forested areas into urban landscapes or agricultural land leads to habitat loss, fragmentation, and the disruption of ecological processes (Ribeiro et al., 2011; Zemp et al., 2017). These anthropogenic activities significantly affect biodiversity conservation, ecosystem functioning, and sustainable land use (Barlow et al., 2016; Rocha-Santos et al., 2020). While extensive research has focused on deforestation in the Amazon rainforest due to its profound impact on global climate and biodiversity (Zemp et al., 2017; Ferrante and Fearnside, 2020; Silva Junior et al., 2021), it is essential to recognise the ecological, economic, and social importance of forests in other regions (Myers et al., 2000; Hamilton and Friess, 2018). However, there are also natural-based drivers of forest and vegetation loss, like fire regimes and browning due to severe and prolonged droughts (Garreaud et al., 2020; Miranda et al., 2020; Smith-Ramírez et al., 2022).

At the landscape level, severe water deficits over the last decades (Garreaud et al., 2020; Fuentes et al., 2022a), and global warming (Boisier et al., 2016) have led to forest browning (Miranda et al., 2020) and tree mortality in some regions with prolonged droughts (Matskovsky et al., 2021). Likewise, extensive forest fires are increasing in frequency due to climate change, affecting forest ecosystems and plantations in large regions of the globe (Castillo et al., 2020; Canadell et al., 2021; Mansoor et al., 2022), reducing vegetation health and vigour. Since all these processes share a decline in vegetation, disentangling deforestation from other causes of forest degradation becomes challenging (Sebald et al., 2021). However, it is essential for policy-making and management at the landscape level.

Given the urgency in delivering new monitoring strategies to track forest changes, there has been an overtaking development of new advances and technologies that allow the continuous monitoring of forested areas to assess forest changes nationwide rapidly (Hansen et al., 2016). However, synoptic and regular data are needed to achieve a large-scale monitoring approach (Danielsen et al., 2009). Hence, remote sensing data have gained increasing popularity for automatic change detection of Earth's changes as it allows the periodic monitoring of the surface characteristics (Fuentes et al., 2019; Japitana and Burce, 2019; Weiss et al., 2020; Fuentes et al., 2022b, 2024). For example, optical satellites with multispectral instruments evaluate changes within the visible and near-infrared wavelength range of the electromagnetic spectrum (Thakur et al., 2020; McAllister et al., 2022), while radar satellites use microwave wavelengths (Karthikeyan et al., 2020), offering the advantage of cloud penetration and monitoring during all seasons (Kerr et al., 2001; Filipponi, 2019). Machine learning, segmentation, or statistical approaches have been commonly used to assess changes and tendencies in remotely sensed time series data (Lary et al., 2016; Yin et al., 2018).

Different methods employ distinct architectures to trace breaks or changes in forest time series data (Zhu, 2017; Housman et al., 2018; Asokan and Anitha, 2019). In many cases, changes must demonstrate continuity/consistency within the time series and not simply represent a single anomaly, which could be caused by clouds, cloud shadows, floods, or artefacts in satellite scenes (Puhm et al., 2020). Detecting consecutive outliers can ensure the presence of a structural break in the time series, but this often leads to a delay in precisely defining the break, hindering real-time change detection (Verbesselt et al., 2011). Structural breaks can be defined as statistically significant changes in time series, implying changes in trend, mean, or variance (Muthuramu and Maheswari, 2019; Loginova and Mann, 2022), and may result in the temporal segmentation of a time series (Pasquarella et al., 2022). Alternatively, other change detection methodologies may utilise phenological curves that combine multi-annual data into day-of-the-year (DOY) series to detect outliers based on observations within the same season, considering historical observations of a particular month or week instead of consecutive ordinal observations. These approaches require prior knowledge of vegetation behaviour during a period of non-disturbance and seasonal climatic conditions (Estay and Chávez, 2018; Zeng et al., 2020), especially as interannual phenological variation changes between vegetation types (Lopatin, 2023) and thus can affect the stability of the approach.

Several algorithms for land change detection have been tested in deforestation studies. Cai et al. (2023) applied the continuous change detection and classification (CCDC) algorithm to track forest changes with high accuracies. Schultz et al. (2016) applied the break detection for satellite time series data (BFAST) in combination with different vegetation indices to track deforestation with robust results. Similarly, Schultz et al. (2015) evaluated error sources in deforestation detection using BFAST, highlighting the necessity of fine-tuning the algorithm in some areas. LandTrendR is another temporal segmentation algorithm that has proven proficient in tracking annual forest disturbances (Cohen et al., 2018; Pasquarella et al., 2022). The vegetation change tracker (VCT) algorithm has also been developed to track forest disturbances with annual or biannual satellite data (Huang et al., 2010) and has been tested for deforestation in the Yunnan province of China, with accuracies of up to 82.7% (Pang et al., 2013). However, little consensus has been found in the results of all these change detection methods. Cohen et al. (2017) compared different change detection algorithms considering the full range of forest disturbance magnitudes and found disagreement on the spatial disturbance occurrences between algorithms. While most unsupervised change detection alternatives have proven accurate in depicting overall vegetation changes (Zhu and Woodcock, 2014; Estay and Chávez, 2018; Wu et al., 2020), less attention has been paid to assessing

Table 1
Proportion of natural vegetation types and plantations in the study region.

Class	Area (km^2)	Coverage (%)
Deciduous forest	9,276.5	11.9
Sclerophyllous forest	29,198.9	37.4
Thorny forest	15,525.1	19.9
Altitude grassland	2,684.2	3.4
Altitude low shrubs	11,423.4	14.6
Sclerophyllous shrubs	2,474.4	3.2
Thorny shrubs	1,555.3	2.0
Plantations[a]	6,168.0	7.9
Bareland	5,621.4	7.2

[a] Natural vegetation corresponds to potential habitat distributions. Therefore, coverage including plantations should exceed 100%.

if their sole use is proficient for separating deforestation from other sources of forest decay. As a consequence, Cohen et al. (2018) underscored the necessity of a secondary classification to improve disturbance detection.

Different studies have highlighted the challenge of distinguishing deforestation from other causes of forest deterioration. For instance, when studying forest cover changes from satellite imagery, Hansen et al. (2013) refer to the "proximate" causes of disturbances. Other studies directly assess the contribution of climate- and human-based variables in forest productivity or net primary productivity (Chen et al., 2021). Likewise, approaches involving field observations are also used to assess the contribution of drivers of change (Redlich et al., 2022), although they may be difficult to scale up to the landscape level. However, incipient citizen science alternatives have been implemented to address this scaling issue (Arcanjo et al., 2016). For example, Sebald et al. (2021) incorporated the landscape context by estimating the cumulative disturbed forest area surrounding forest patches in a secondary classification to identify causal agents of disturbance, resulting in an improved depiction of real deforestation. However, few examples of these human- and natural-based drives of vegetation change remain, and robust methods are still needed to operationally depict deforestation from other drivers of forest change at multiple spatial scales.

The primary objective of this study is to disentangle deforestation from other forest degradation causes with the aim of detecting near real-time human-induced deforestation using satellite data, including time series. To achieve this, we seek (a) to evaluate and compare three architecturally different algorithms of change detection in forest monitoring, discussing their advantages and challenges; (b) to apply a secondary classification to distinguish deforestation from other forest disturbances, such as large-scale fires and droughts, utilising the outputs of the change detection algorithm and ancillary data; (c) to compare deforestation results against governmental inspection requests raised by the community, evaluating the appropriateness of these requests and the temporal gap between them. We will use a large portion of central Chile as a study site to achieve these objectives. Central Chile has undergone severe droughts and fires over the last decade, presenting alarming tree mortality increases in a complex landscape of forestry and agriculture mosaics (Garreaud et al., 2020; Miranda et al., 2020; Fuentes et al., 2021).

2. Materials and methods

2.1. Study region

To address our research goals, we selected central Chile between the Valparaiso and El Maule regions (−32.3°−−36.5° S; Fig. 1), an area with an extent of about 78,000 km^2. Forests in this region are important, as they have been acknowledged as one of the world's biodiversity hotspots (Myers et al., 2000). This region is mainly dominated by Mediterranean climate types (Csa and Csb) according to the Köppen–Geiger climate classification (Sarricolea et al., 2017; Beck et al., 2018) and has historically experienced important land cover changes (Montoya-Tangarife et al., 2017; Miranda et al., 2017; Fuentes et al., 2021). Moreover, these forests face multiple threats, including urban and peri-urban expansion, agriculture expansion, and the establishment of exotic plantations (Manuschevich, 2018). Consequently, according to the International Union of Conservation of Nature (IUCN) (Alaniz et al., 2016), most of these ecosystems have been classified as threatened. Furthermore, these ecosystems have experienced severe and prolonged drought conditions, resulting in "browning" events (Garreaud et al., 2020; Miranda et al., 2020). Additionally, the region has witnessed large-scale wildfire events over the past decade (Smith-Ramírez et al., 2022).

Vegetation formation classes in the study region and their extent are in Table 1. Forests in the region encompass various vegetation types (Cowling et al., 1996) predominantly dominated by sclerophyllous species. Thorny scrublands, mainly characterised by *Vachellia caven*, are also present, along with deciduous forests of *Nothofagus* species in southern areas with higher precipitation (Donoso and Donoso, 2007; Salas et al., 2016). Sclerophyllous forest formations are characterised by evergreen trees with hard leaves that reduce water loss. These traits make the chlorophyll vegetation resilient to water stress and drought (Yin and Bauerle, 2017). Plantations and other land cover classes overlap these categories (Zhao et al., 2016). This study includes forest categories from Table 1 but also incorporates plantation in the analysis.

2.2. Datasets and pre-processing

We used the Landsat constellation, including Level 2 Collection 2 tier 1 scenes from TM, ETM+, and OLI/TIRS sensors for Landsat 5, 7, 8, and 9 (USGS, 2022). These data included 8,804 scenes from 2000-01-01 to 2022-06-01. We merged the different collections using cloud and shadow masks based on the QA_PIXEL band information of the CFMASK algorithm (Foga et al., 2017).

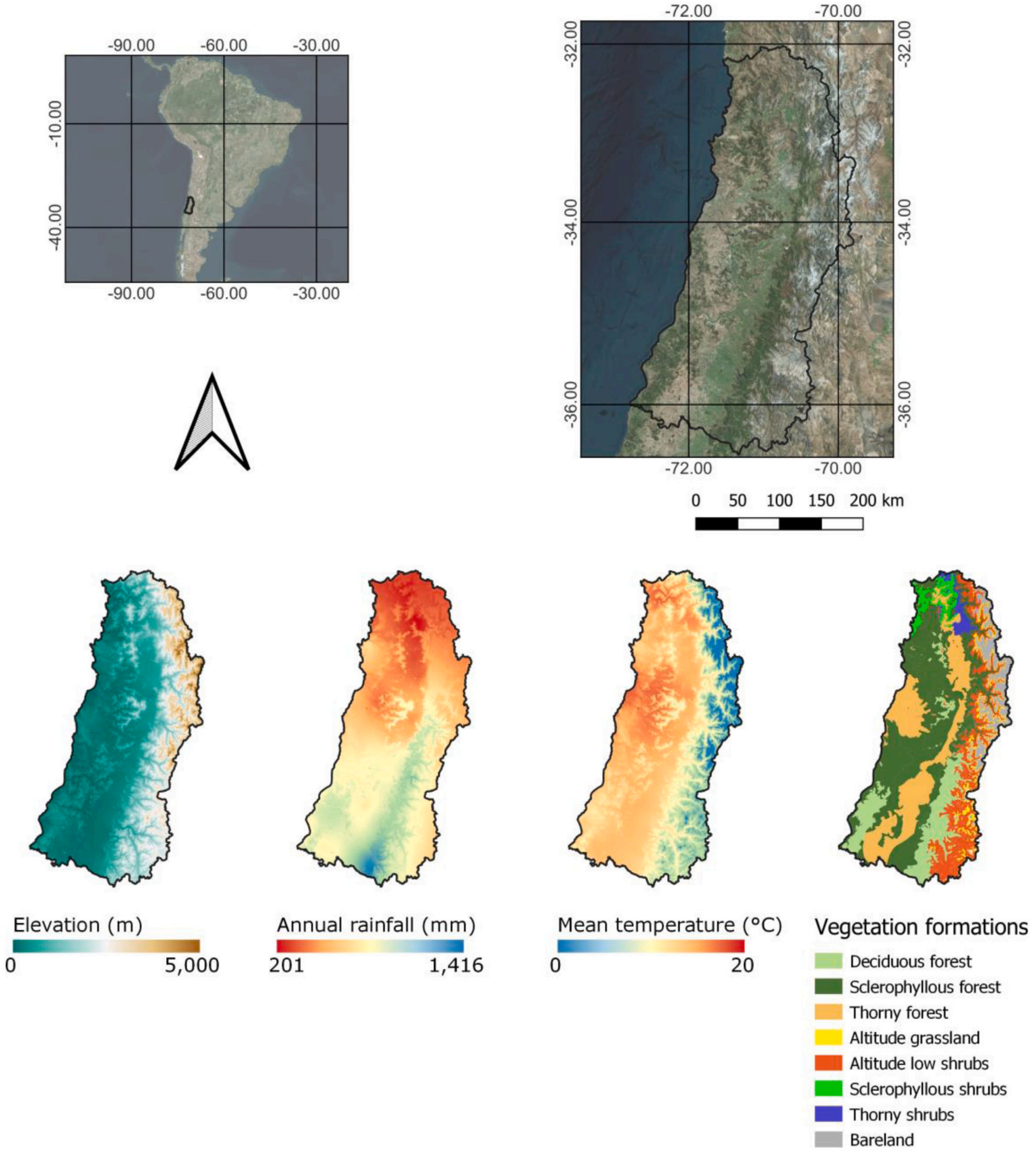

Fig. 1. Study region and its main characteristics in terms of elevation, mean annual rainfall and temperatures, and vegetation formation classes.

We depicted the normalised difference vegetation index (NDVI) (Rouse et al., 1973) of the image collections using the red and near-infrared bands of images. We further used the 2014 land cover map developed by Zhao et al. (2016) in the post-processing step to limit changes detected in forests, plantations, or shrubland areas, avoiding agricultural lands that can present artificial structural changes due to management. Additionally, we included elevation data from the Multi-Error-Removed Improved-Terrain digital elevation model, which was included as a covariate in the secondary classification step alongside the slope of the terrain calculated from it.

We also used calibrated and ortho-corrected Ground Range Detected scenes from synthetic aperture radar Sentinel 1 satellites from February 2016 to July 2022. These were filtered based on the Interferometric Wide Swath (IWS) mode using a descending orbit direction, since it allowed to maximise the number of scenes. The back-scatter intensity from dual-polarimetric Sentinel-1 images was used to calculate the Radar Vegetation Index (Mandal et al., 2020) using:

$$RVI = \frac{4\sigma^0_{VH}}{\sigma^0_{VH} + \sigma^0_{VV}} \tag{1}$$

being σ^0_{VH} and σ^0_{VV} the dual cross polarisation (vertical transmit/horizontal receive) and single co-polarisation (vertical transmit/vertical receive) backscatter intensity bands, respectively. This collection was used to obtain some covariates in the secondary classification step.

We used Google Earth Engine (Gorelick et al., 2017) and the Data Cube Chile (https://datacubechile.cl/) to acquire and process the data. Subsequent methodologies and analyses were carried out using Python ≥ 3.7.

2.3. Unsupervised change detection

We selected three algorithms belonging to structurally different approaches to evaluate methodologies to trace structural changes in heterogeneous and complex forest ecosystems in Central Chile. We tested: (1) a probabilistic approach based on the phenological characterisation of vegetation considering a bivariate time series based on day-of-the-year data; (2) a temporal segmentation method assuming the decomposition of time series in intra-annual, inter-annual, and structural changes by evaluating the deviation of observations and predictions based on ordinary least squares regressions. This method uses bivariate/multivariate data containing as reference the date; and (3) a temporal segmentation based on the optimisation of a cost function, where the cost is additive in the segmented blocks and requiring a univariate/multivariate time series, relaxing the need for temporal references for the change-point detection.

The outputs of these algorithms correspond to change dates and magnitudes. The change magnitudes were calculated as the difference between average NDVI values within stable periods adjacent to the detected changes.

Phenological characterisation: the non-parametric phenological cycle and anomaly detection (npphen) algorithm

The first algorithm implies using multi-year phenological stages in forests to characterise the behaviour of phenological curves. We used the methodology defined by the 'npphen' R-package (Estay and Chávez, 2018). This methodology uses multi-annual information and orders them to day-of-the-year (DOY) to have a single phenological curve (or a pseudo-DOY in the case of the southern hemisphere). This curve is fitted using Kernel Density Estimation (KDE). This allows us to depict a generic phenological response per pixel as:

$$\hat{f}(x;H) = \frac{1}{n}\sum_{i=1}^{n} K_H(x - X_i) \tag{2}$$

where X corresponds to a time series containing paired values of vegetation indices and the DOY, being X_i the pair of values for the i_{th} observation, n corresponds to the number of observations, which can be calculated as the multiplication of the number of annual phenological cycles by the observations per cycle, x is a generic point in the paired values, H is the bandwidth 2×2 array, K is the kernel, in this case corresponding to a Gaussian kernel of size defined by H (Wand and Jones, 1994), being *f(x)* the bivariate density function of X.

Npphen can lead to anomaly detection of present values when compared to the historical trend of that time of the year (e.g., weekly) using a probabilistic approach based on the following:

$$A_i = VI_{obs} - VI_{exp} \tag{3}$$

being A_i the anomaly for the i_{th} DOY, VI_{obs} the observed vegetation index and VI_{exp} the expected vegetation index for that DOY.

We fitted npphen for the period 2000–2015 using the Landsat collection to set each pixel's historical phenological response, consequently estimating anomaly probabilities from 2016 (i.e., see Section 2.4). We defined a structural break in the time series when at least five consecutive negative anomalies exceeded two standard deviations of the "training" data. We did this assuming that negative changes or perturbations in forest and shrublands structure cause a decline of NDVI values (Hudak and Wessman, 2000) and to avoid single anomalies that may be caused by artefacts that could obscure the structural break detection. By using npphen, only the initial change detected is considered, as anomalies in the time series persist until the signal aligns with a pattern similar to the undisturbed period.

Temporal segmentation: the continuous change detection and classification (CCDC) algorithm

The second method for defining structural breaks is the Continuous Change Detection and Classification (CCDC) algorithm, originally defined to trace land cover changes (Zhu and Woodcock, 2014). The algorithm is used in time series composed by seasonality, trends, and breaks, estimating coefficients through ordinary least squares (OLS) and fitting harmonic functions as:

$$\hat{\rho}(i,x)_{OLS} = a_{0,i} + a_{1,i}cos(\frac{2\pi}{T}x) + b_{1,i}sin(\frac{2\pi}{T}x) + c_{1,i}x \tag{4}$$

being x, constrained to the following boundaries:

$$\tau^*_{k-1} < x \le \tau^*_k \tag{5}$$

where $\hat{\rho}(i,x)_{OLS}$ is the estimated value of the time series for the x_{th} day of the year; i correspond to the dimension of the time series evaluated (band of images); T is the number of days per year; $a_{0,i}$; $a_{1,i}$, $b_{1,i}$; and $c_{1,i}$ are the overall (mean), intra-annual change (seasonal), and inter-annual (trend) change coefficients for the i band, respectively; and τ^*_k are the kth break points.

CCDC can use single or multiband images for change detection and seeks to detect breaks by evaluating the difference between observations and predictions, normalised by the root mean square error (RMSE) during a defined time window, as:

$$\frac{1}{k}\sum_{i=1}^{k}\frac{|\rho(i,x)-\hat{\rho}(i,x)_{OLS}|}{n\times RMSE_i} > 1(z \text{ consecutive times}) \tag{6}$$

where k is the number of bands used, n is a factor that multiplies the RMSE for the selection of the break based on the assumption of model prediction ranges, defined as 3 in this case, and z represents consecutive observations where errors exceed n times the RMSE to trace the break. We used the Google Earth Engine implementation, and tested several chi-square probability thresholds, setting z to 5 and a chi-square probability threshold to 0.9 to improve the change detection (Supplementary materials; Figure S1).

Temporal segmentation: linearly penalised segmentation (PELT)

We selected the Pruned Exact Linear Time (PELT) algorithm as the third methodology, which is a linearly penalised segmentation implemented in the '*Ruptures*' Python library (Truong et al., 2020). PELT efficiently deals with an unknown number of breaks in each time series. In a time series defined by $y_{1:n}$ of size n, and m change points at $\tau_{1:m}$ dates, structural breaks can be identified by minimising the following (Wambui et al., 2015):

$$\sum_{i=1}^{m+1}[l(y_{(\tau_{i-1}+1):\tau_i})+\beta] \tag{7}$$

being l the cost function for the ith segment, and β corresponds to a penalty to minimise over-fitting.

PELT mixes partitioning and pruning to achieve computational efficiency by applying the optimal solution $F(n)$ of Eq. (7):

$$F(n)=\min_{\tau_m}\{F(\tau_m)+l(y_{(\tau_m+1):n})\} \tag{8}$$

being the inner minimisation $F(\tau_m)$:

$$F(\tau_m)=\min_{\tau|\tau_m}\{\sum_{i=1}^{m}[l(y_{(\tau_{i-1}+1):\tau_i})+\beta]\} \tag{9}$$

We used a radial basis function as model input, setting the minimum distance between change points to 3, the subsample to 5, and the penalty to 30 since it allowed us to empirically improve the change detection performance through accuracy metrics (Supplementary materials; Figure S1).

2.4. Algorithm performance and timeliness analysis

We used the Global Forest Watch (GFW) map of deforestation records (https://www.globalforestwatch.org/) to initially select potential areas of forest change between 2016 and 2022. We then corroborated the validation sites by visually interpreting Google Earth Pro images. We selected a total of 382 validation sites, from which 142 corresponded to human-based deforestation and 147 to other changes, i.e., 91 polygons associated with severe drought conditions during the summer of 2019–2020 that led to vegetation "browning" in the studied region as reported by Miranda et al. (2020) and 56 polygons were selected as affected by fires. We also selected 93 sites with stable time series where no changes occurred. We used pixel-based data for the analyses, thus having several time series per site (i.e., 23,053 pixel-based time series in total). The selected time frame of analysis was chosen to minimise error in methods needing historical data before validation, as npphen, and because of the higher frequency of high resolution images available in Google Earth, which facilitates the selection of reference polygons for validation. Five examples of non-deforested (above) and deforested (below) reference polygons and background reflectance images for the years 2016 and 2021 are shown in Fig. 2. For the reader's convenience, Sentinel 2 images are displayed instead of Landsat images.

We evaluated the performance of the three algorithms in terms of consumer's accuracy (CA), producer's accuracy (PA), F1-score, overall accuracy (OA), and Cohen's Kappa coefficient as suggested by Olofsson et al. (2014), being PA estimated as the ratio between correctly classified pixels in each category and the number of reference pixels within that category, while CA are correctly classified pixels in each category divided by the number of pixels classified as such within that category. Additionally, OA is calculated as:

$$OA=\frac{tp+tn}{tp+fn+tn+fp} \tag{10}$$

being tp, tn, fp, fn true positive, true negative, false positive, and false negative observations, respectively. Kappa coefficient is estimated using:

$$kappa=\frac{P_o-P_e}{1-P_e} \tag{11}$$

being P_o the probability of actual agreement and P_e the probability of a random agreement. Lastly, the F1-score is calculated using:

$$F1=2\times\frac{precision\times recall}{precision+recall} \tag{12}$$

being precision and recall estimated as:

$$precision=\frac{tp}{tp+fp} \tag{13}$$

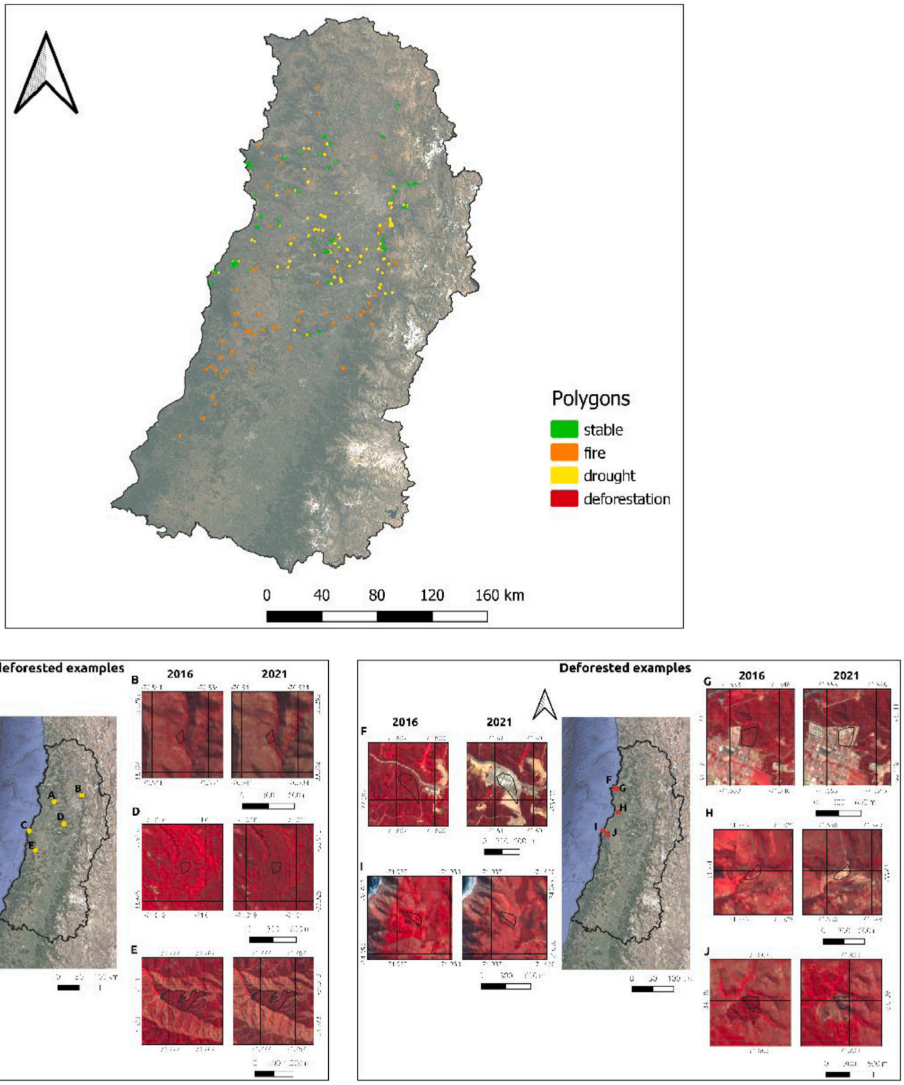

Fig. 2. Reference polygons used in this study (above) and examples of non-deforested (below left) and deforested (below right) forest ecosystems between 2016 and 2022. Black polygons depict validation polygons. A, B, and C show sites without human- and natural-based changes, while D was classified as affected by drought due to the browning observed, and E was classified as affected by fires in 2017 through high-resolution satellite images from Google Earth Pro (spatial resolution of less than 10 m).

$$recall = \frac{tp}{tp + fn} \tag{14}$$

and implying the ability of algorithms to avoid false positives and to identify positives, respectively.

We finally assessed the model performances of:

1. all deforested (human-made) areas against stable (undisturbed) forest areas;
2. all deforested (human-made) areas against stable and natural-made changes (stable+droughts+fire);
3. same as comparisons (1) and (2), but separating natural forest and plantation deforested areas.

We divided the analysis into these sections to assess the ability of the unsupervised change detection algorithms to depict only deforestation (human-based changes) across vegetation types and natural forest alterations.

Additionally, the rate of algorithm deforestation detection was evaluated in 15 randomly selected reference polygons including both, native vegetation and plantations. The reference date of deforestation was selected by visually interpreting the first Landsat image where deforestation was evident. The temporal lag of deforestation detection was calculated as the difference between the

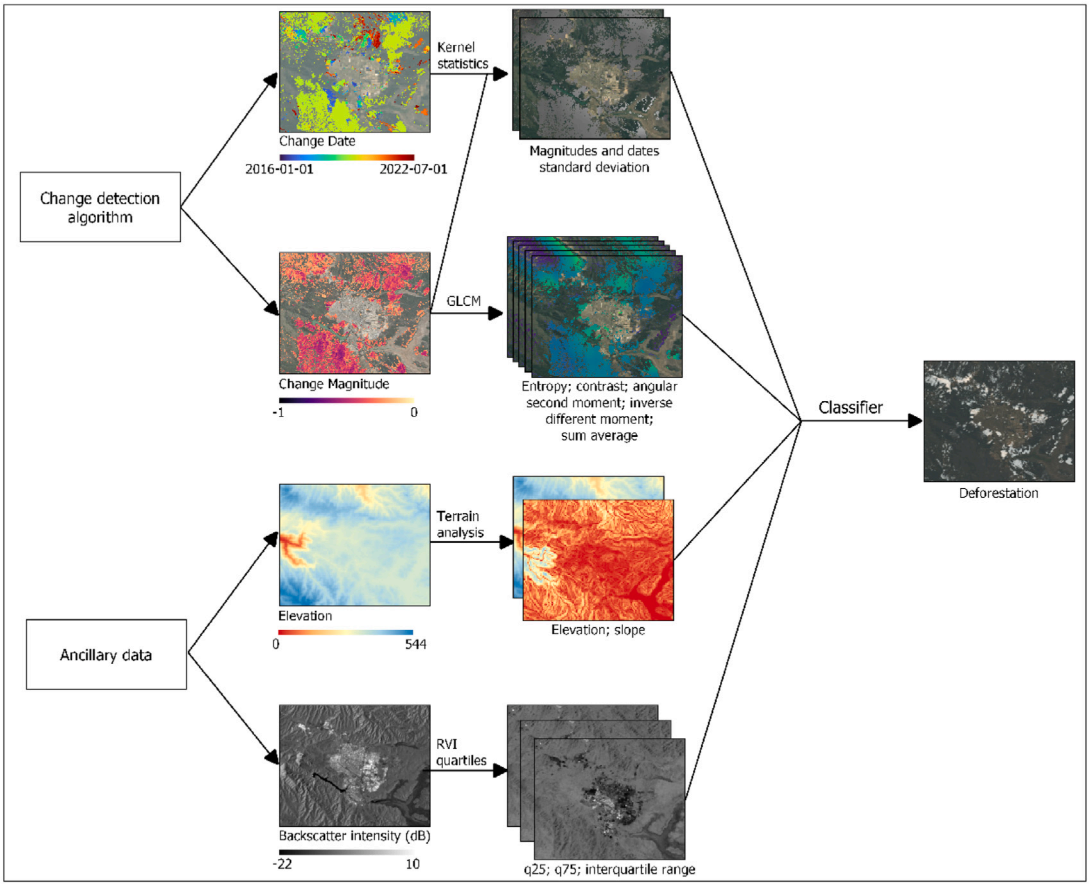

Fig. 3. Schema depicting the workflow of the methodology for distinguishing deforestation from other natural-induced changes.

algorithm detection date and the reference date. This aims to depict not only the models' accuracy but also their stability and lag time of response to achieve their accuracy.

2.5. Disentangling deforestation from other natural changes

A supervised classification approach was used to depict deforestation from natural changes in the landscape. To achieve that, we utilised the best of the three unsupervised change detection algorithms in terms of accuracy and fast lag response. We masked out pixels with positive change magnitudes as we assumed that all deforestation and natural alteration would decrease NDVI values. We then used the spatial patterns of the binary detection and its magnitudes to assess if the changes originated from deforestation or natural drivers.

We assumed that vegetation changes associated with droughts and fires lead to broad and heterogeneous spatial patterns across the landscape. Contrarily, anthropic deforestation, like logging and urban expansion, is expected to have large change magnitude with smaller and homogeneous spatial extents. Therefore, we used the gray level co-occurrence matrix (GLCM) (Haralick et al., 1973) approach to generate textural features from the magnitude of changes using square kernel neighbourhoods of 15 × 15 pixels. Likewise, we calculated the neighbourhood variations using the standard deviation of the change dates and magnitudes within a square kernel of 50 × 50 pixels. The selected kernel dimensions were chosen because they yielded the best results compared with other configurations explored. We used the entropy, contrast, inverse difference moment (IDM), angular second moment (ASM), and sum average (SA) layer metrics from the GLCM analysis. Entropy signifies the degree of complexity in the spatial distribution of pixels, contrast reflects the local intensity variations between neighbouring pixels, IDM illustrates the local homogeneity, ASM measures the uniformity or smoothness of an image, while SA represents the average intensity of the sum of pixel pairs. We combined the GLCM data with change magnitudes and the standard deviation layers derived from the outputs of the selected unsupervised algorithm as predictors for the supervised classification (Fig. 3). Additionally, slope and elevation were also included as predictors, along with the interquartile range and the 25th and 75th quartiles of RVI images as RVI has been recognised as an alternative for monitoring vegetation growth (Nasirzadehdizaji et al., 2019), and the interquartile range represents a measure of growth variability.

Table 2
Performances of the three unsupervised change detection algorithms, with metrics estimated between deforested and stable reference classes and between deforested and all other classes (stable, drought-affected, and fire-affected). The comparison was performed on every time series (combined) and for native vegetation and plantations separately. Bold numbers depict local maxima in the models.

Forest	Algorithm	OA[a]	PA	CA	kappa	f1	OA	PA	CA	kappa	f1
		Stable v/s deforested					All v/s deforested				
Native	*npphen*	**0.83**	**0.83**	**0.83**	**0.67**	**0.84**	0.39	0.57	0.53	0.05	0.24
	CCDC	0.78	0.78	0.78	0.56	0.81	0.27	0.50	0.50	0.03	0.23
	PELT	0.78	0.78	0.79	0.57	0.76	**0.55**	**0.60**	**0.54**	**0.09**	**0.27**
Plantation	*npphen*	0.96	0.97	0.88	0.85	0.97	**0.61**	**0.64**	0.71	**0.27**	**0.68**
	CCDC	0.95	0.93	**0.97**	0.87	0.98	0.53	0.58	0.69	0.14	0.64
	PELT	**0.99**	**0.98**	0.96	**0.95**	**0.99**	0.55	0.59	**0.73**	0.18	0.66
Combined	*npphen*	0.89	0.90	**0.87**	0.76	0.92	0.48	0.61	0.61	0.15	0.46
	CCDC	0.88	0.86	0.86	0.71	0.92	0.37	0.55	0.57	0.06	0.41
	PELT	**0.90**	**0.91**	0.86	**0.77**	**0.93**	**0.55**	**0.66**	**0.63**	**0.21**	**0.49**

[a] OA: Overall accuracy; PA: Producer's accuracy (mean of classes); CA: Consumer's accuracy (mean of classes).

The reference polygons were split into a 10% for validation (2283 pixels), while a 10-fold cross-validation was applied on the remaining 90% polygons. We used the Random Forest algorithm with 150 trees and an out-of-bag fraction of 0.5 to train a pixel-based classifier to depict deforestation from other changes and to differentiate forest disturbance sources since these parameters resulted in a good performance using a grid search based on the validation subset.

2.6. Independent verification via citizen science

Finally, we used the citizen-based complaints from the *Superintendencia del Medio Ambiente*, the organism from the Ministry of Environment in charge of monitoring the natural resources, to filter 16 *in-situ* descriptions containing the words "*forest", "fell*", "cut*down", and "sclerophyllous". Complaints were also filtered based on forests, shrublands, and plantation land cover classes from the Zhao et al. (2016) map. These complaints (Supplementary materials, Table S1) were compared with deforestation maps, and the dates of the change detection were used as an independent verification of the method.

3. Results

3.1. Performance of unsupervised change detection methods

Table 2 presents the performance of different change detection algorithms used between stable (i.e., no changes between 2016–2022) and deforested classes and between all other classes (stable, fire, and drought affected) and deforested classes. The algorithms show robust performances when comparing stable and deforested classes, with OA ranging from 0.78 to 0.99 and kappa coefficients from 0.56 to 0.95. Under native forest types, npphen outperforms other algorithms, but under plantations, PELT has the best performance. Likewise, when combining native vegetation and plantations, PELT slightly outperforms other algorithms. Overall, we observed that all algorithms perform less accurately on native forests than on plantations, given the vegetation heterogeneity. In general, commission errors are slightly higher than omission errors, which is reflected in slightly lower CA (CA = 100 - commission errors) compared to PA (PA = 100 - omission errors).

We depicted very low accuracies when comparing deforestation with the rest of the categories (including natural-based changes), with OA and kappa values ranging from 0.27 to 0.61 and from 0.03 to 0.27, respectively. However, again plantations show a better performance than native forest types. In this case, large errors are caused, among others, by natural-induced changes detected by algorithms other than deforestation, implying that further processing is required to distinguish between human- and natural-induced vegetation changes.

Fig. 4 shows the averaged NDVI time series for non-deforested (left) and deforested (right) examples with their corresponding change detection by the tree algorithms (vertical lines). PELT and CCDC algorithms depicted a structural change in the summer of 2020 associated with drought in Fig. 4D. All three algorithms detect a fire-based change in example E from Fig. 4 during 2017.

Deforested examples (right-column panel of Fig. 4) are correctly identified by PELT and CCDC algorithms in all cases. On the other hand, npphen detects structural changes in four of the five examples. Example I is associated with a change in vegetation in the period used for training the algorithm (2000–2016). In this example, a growing forest can be observed between 2008 and 2014, being the previous years characterised by early-stage forest vegetation. This results in the spread of NDVI low-probabilities observed in the phenological curve of example I (Supplementary materials, Figure S3), affecting the change detection.

Fig. 5 shows spatiotemporal maps of structural breaks since 2016, applying a 100–200 m buffer around the example polygons. The npphen algorithm tracked deforestation changes, except for example I, incurring in more false negatives. Poorly defined boundaries for phenological curves (Figure S3 associated with vegetation changes between 2000 and 2016, i.e. training period in npphen) limit phenology-based algorithms' structural breaks detection capacities, preventing structural breaks tracking in Fig. 5 example I. On the other hand, CCDC and PELT changes are correctly delimited.

Changes in non-deforested examples only occur within example D (Fig. 5) using PELT, corresponding to a drought event (Fig. 4). Meanwhile, example E, corresponding to a fire event, was identified by all unsupervised algorithms. CCDC detected changes in sparse pixels from examples C and D, but most pixels in those cases do not present changes.

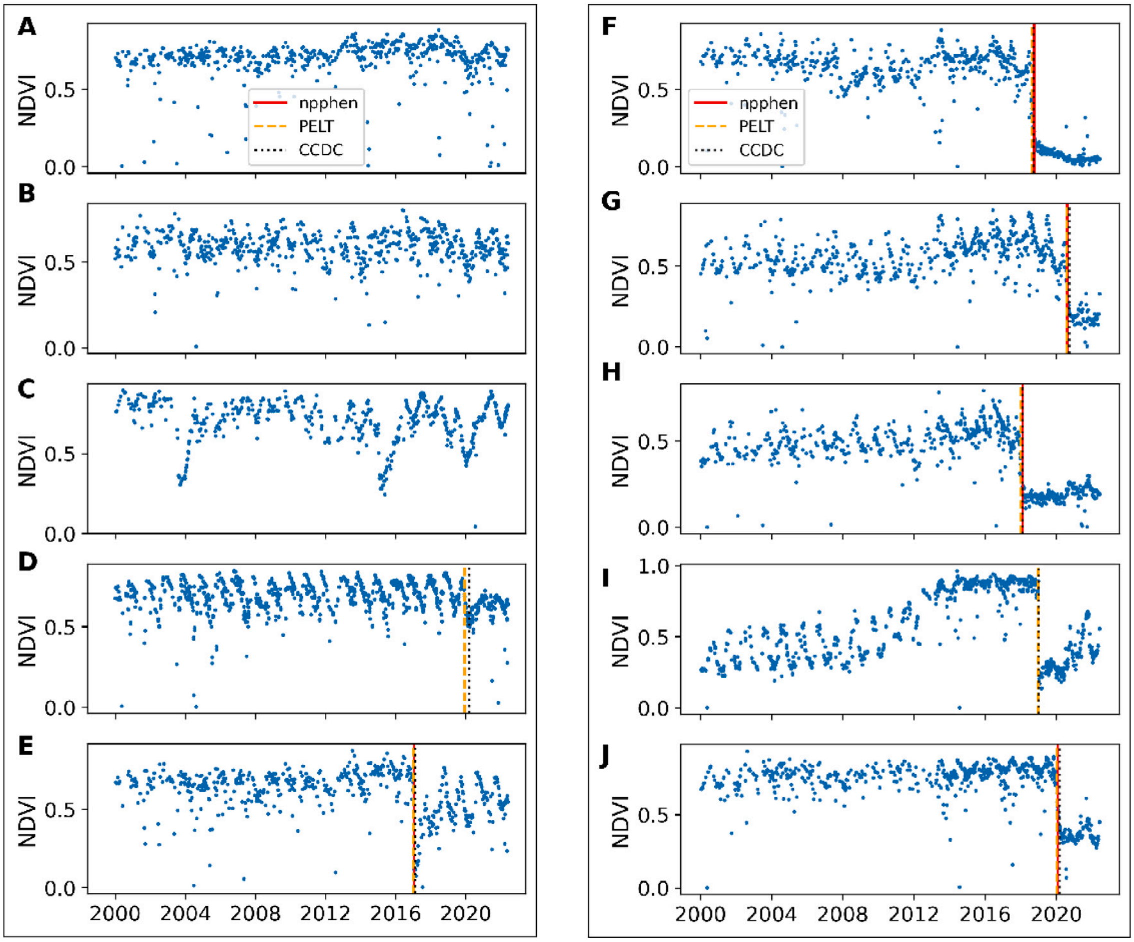

Fig. 4. Non-deforested (left) and deforested (right) averaged NDVI pixels sampled from reference examples. Structural changes detected using npphen, CCDC, and PELT algorithms are also presented (vertical lines). A, B, and C polygons were classified as stable, while D and E were classified as affected by drought and fires, respectively. F-J polygons are classified as deforested.

3.2. Latency between reference deforestation and change detection

The temporal lag between reference deforestation dates and average change detection dates is shown in Fig. 6. Although PELT leads to the best cumulative change detection, it also presents the most extended temporal lag (in percentage) between average change detection and reference deforestation dates. While PELT deforestation dates in Fig. 4 are accurately tracked, its cost function optimisation results in several months of delay in tracking changes, making it more suitable for offline applications. In contrast, CCDC demonstrates the fastest detection response, with over 50% of pixel changes detected within the first two months after the reference deforestation date. This lagged response may also be adjusted by modifying z in Eq. (5). CCDC is followed by npphen in the latency between reference deforestation dates and the algorithm detection dates. Thus, the latency of CCDC and npphen makes them suitable for near real-time applications. Given the high performance and fast response of CCDC to depict forest changes, we selected it for the secondary classification step.

3.3. Disentangling deforestation and performance

Fig. 7 shows the date and magnitude of general changes across central Chile. The landscape changes depicted distinct patterns of natural- and human-based changes. For example, the above-zoomed area represents natural changes associated with browning and fire. Here, the changes are widespread with heterogeneous shapes and low change intensities. Contrary, the under-zoomed area depicts deforestation or human-made alteration in the landscape. These changes have unnatural homogeneous shapes, like squares and rectangles, and often high change magnitudes.

Change and magnitude distribution differences between disturbed classes are in Fig. 8. A bimodal distribution of change magnitudes is observed (upper panel) and a large dispersion (middle panel) of change dates that increases during the spring

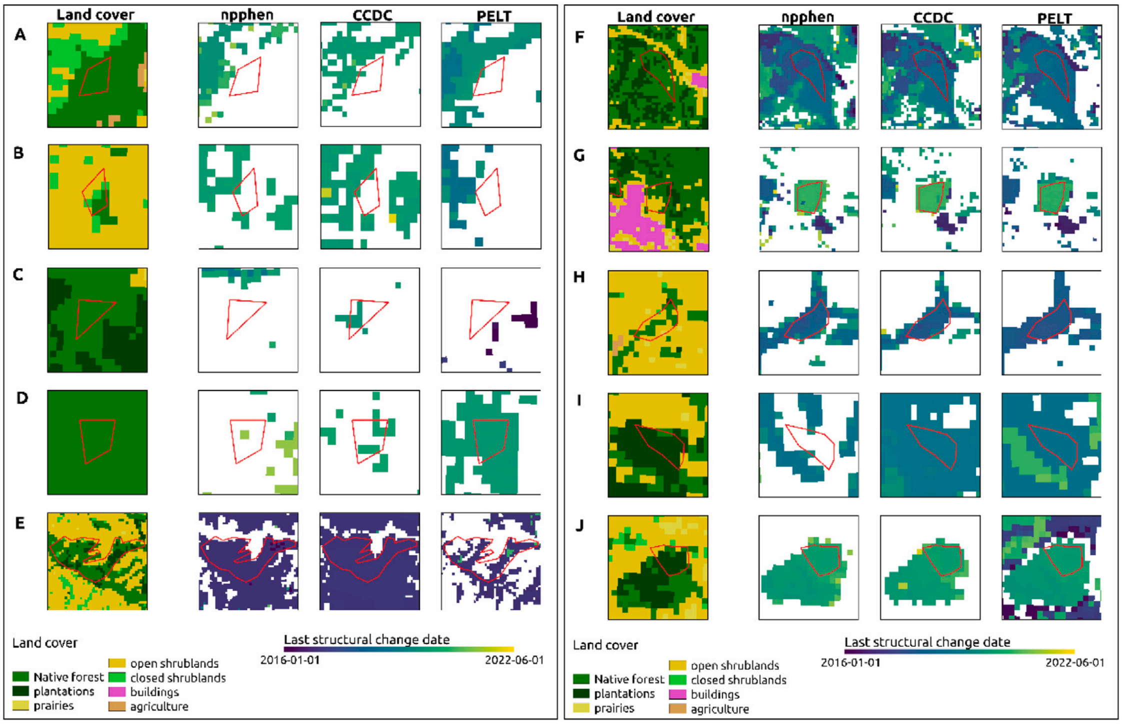

Fig. 5. Spatio-temporal maps of last break detections using three approaches for non-deforested (left) and deforested (right) polygon examples. Letters A-J correspond to non-deforested/deforested example polygons as shown in Fig. 2. Red polygons depict the selected validation areas. Non-deforested A, B, and C polygons were classified as stable, while D and E were classified as affected by drought and fires, respectively. Land cover maps correspond to Zhao et al. (2016).

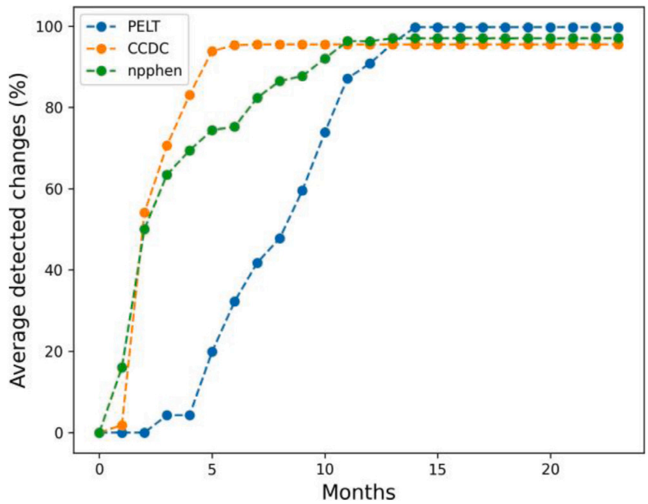

Fig. 6. Temporal lag between reference deforestation and average detected changes using unsupervised algorithms.

and summer seasons. Distinctively larger frequencies were depicted in the summer of 2017, associated with large fire events, and between 2019 and 2020, associated with severe drought conditions (Supplementary materials, Figure S4). We also observed that fires presented the strongest change magnitudes (i.e., lower negative values) followed by deforestation events, while drought events led to higher values. Also, change dates for drought are very limited to specific periods of time, while deforestation and fires showed more spread alteration throughout the study period.

Table 3 show the classification performance using the Random Forest model for disentangling deforestation from other classes and for determining the source of forest disturbance. Results depict a substantial agreement between reference and predicted classes.

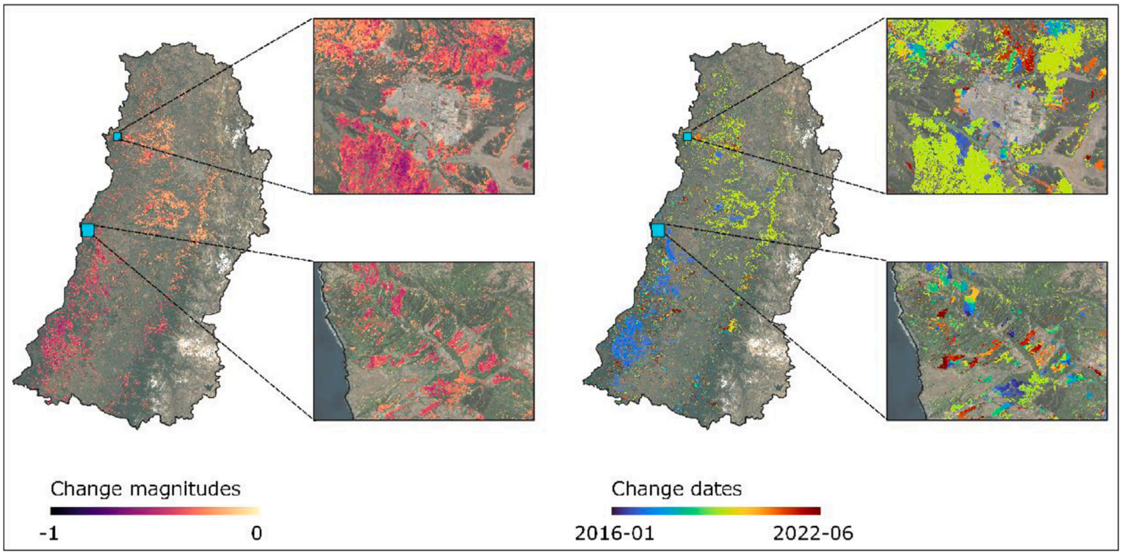

Fig. 7. Change detection magnitudes (left) and dates (right) in central Chile using PELT. Changes correspond to the last break detected on the time series. Two zoomed-in areas are also depicted.

Table 3
Deforestation classification performance using the supervisor Random Forest classifier.

Stage	OA	PA	CA	kappa	f1	OA	PA	CA	kappa	f1
	Deforested v/s nondeforested					Change type				
Calibration	0.99	0.99	0.99	0.99	0.99	0.99	0.99	0.99	0.99	0.99
Validation	0.93	0.92	0.92	0.83	0.92	0.92	0.93	0.92	0.88	0.92

Deforestation is tracked correctly, with similar values for consumer and producer accuracies and a kappa of 0.83 in validation. Additionally, the disturbance sources are also tracked quite correctly, with a kappa value of 0.88 in validation.

The classification results of zoomed-in examples from Fig. 7 are in Fig. 9, showing the changes caused only by deforestation (human-made). False colour images from years 2016 and 2022 are included to evaluate differences, and the mean and standard deviation of deforestation changes depicted from the 10-fold repetitions show stable estimation (i.e., low variations). Likewise, different classes of disturbance sources for the zoomed-in examples evaluated are in Fig. 10.

3.4. Evaluation using citizen complains

Fig. 11 depicts the comparison between user complaints and temporal segmentation algorithms. From the 16 filtered complaints, only 11 presented deforestation events detected (i.e., 69%). However, some of these complaints do not show significant changes in the associated NDVI time series, and in other cases changes are subtle. Furthermore, the methodology often detected forest changes before the occurrence of citizen complaints (Supplementary materials, Figure S5), hence improving the detection in time and space from the *status quo*. Statistically, comparing the complaints where deforestation was detected, the algorithm detection occurs on average 94 days before the complaint is made.

4. Discussion

4.1. Performance of the unsupervised forest change detection algorithms

The PELT temporal segmentation algorithm yielded slightly higher overall accuracies than other algorithms when depicting deforestation against stable vegetation. PELT stands out for its flexibility, as it allows for the adoption of different linear and non-linear models to reduce the cost functions, hence eliminating the need for prior knowledge of seasonal vegetation patterns (Wambui et al., 2015). While PELT is computationally efficient, flexible (Killick et al., 2012), and has demonstrated faster and more consistent performance than visual assessments of breaks in oceanographic wave height time series (Killick et al., 2011), it also demonstrated to work offline, leading to a large lag between deforestation and its detection. On the other hand, changes that occurred during the phenological characterisation using the Landsat collection (2000–2015) affected the results obtained using npphen. By relying on the phenological curve characterization through a period of non-disturbance, npphen leads to the detection of continuous anomalies after a change occurs, making it difficult to detect subsequent changes. These factors reduce its versatility. Nevertheless, these drawbacks

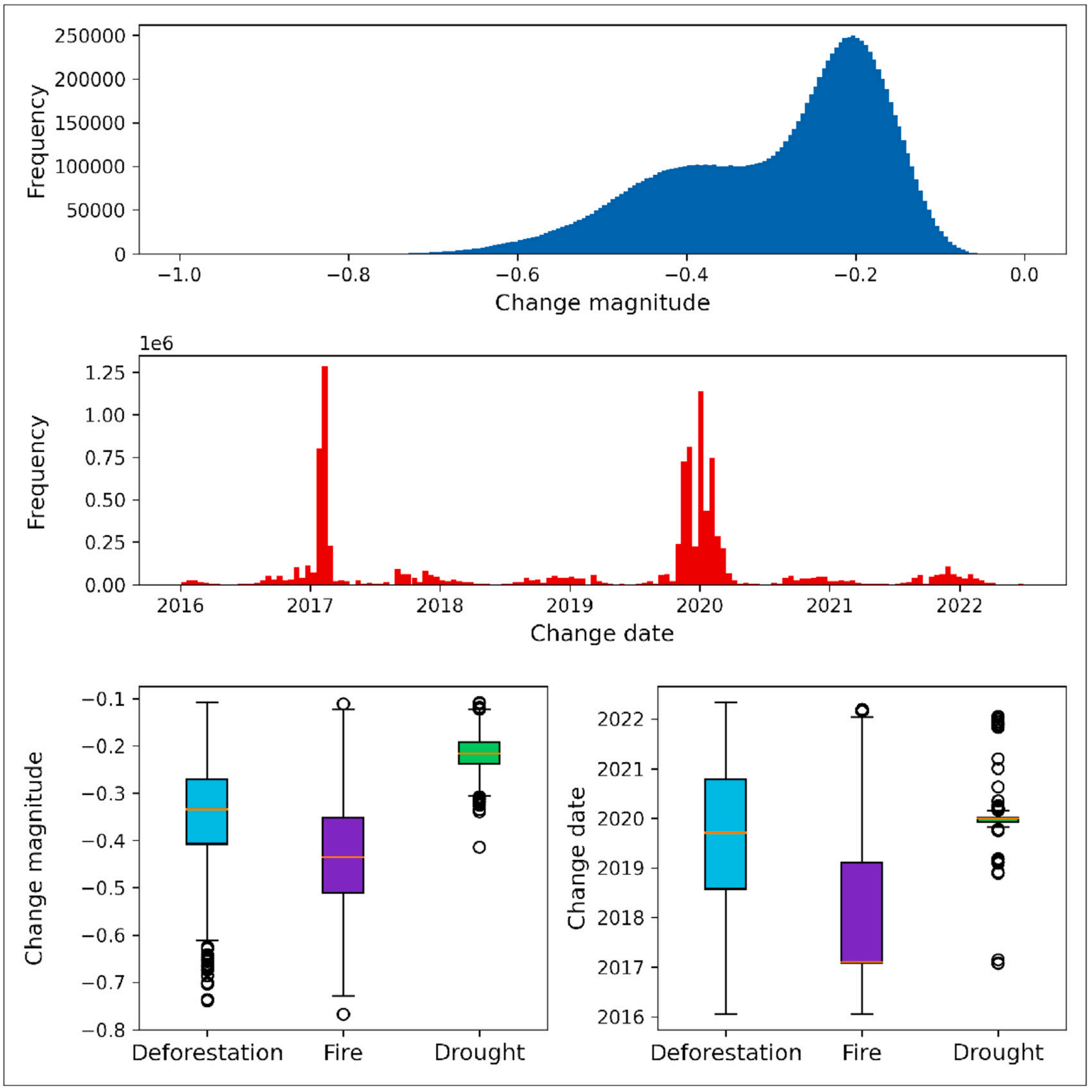

Fig. 8. Distribution of changes based on magnitudes and dates. Histograms of change magnitudes and dates for the entire study region are in the above and middle panels, respectively. The distribution of change magnitudes and dates for reference polygons based on change classes are in the lower panel.

can be mitigated by employing a time series with minimal disturbance during training and selecting only the first change. We make sure to use undisturbed polygons between 2000 and 2015 for evaluating deforestation between 2016 and 2022, except for one reference polygon used for evaluation, which experienced changes during the "training" period (Fig. 4I). This approach has also proven helpful in detecting ecosystems with high dynamic seasonality, such as the blooming desert in northern Chile (Chávez et al., 2019). Unlike npphen, which utilises non-parametric methods and does not assume any predefined phenological cycle shape (Estay and Chávez, 2018), CCDC assumes harmonic/seasonal cycles with different orders among its components (Zhu and Woodcock, 2014). CCDC leads to an overall good performance in the unsupervised change detection and led to the faster deforestation detection response, which implies it may be used for near-real deforestation applications.

The use of different optical satellite datasets can yield varied results due to differences in temporal resolution, the time span of available data, spatial resolution, and the robustness of cloud and shadow detection methods. Notably, we observed noise in the data collections, mainly caused by cloud and shadow detection errors, that increased deviations in the time series (Baret et al., 2007; Griffiths et al., 2020). This, together with artefacts in satellite images such as those caused by the failure of the scan line corrector in Landsat 7, can cause missed structural breaks, impacting npphen and CCDC, which rely on anomaly deviations or deviations of residuals to track significant changes. The frequency of satellite image acquisition also may play a role in timely change detection (Fuentes et al., 2019), and it should be fully considered when aiming for continuous environmental monitoring. For instance, Zhu and Woodcock (2014) highlights the influence of observation frequency on the speed of change detection using temporal segmentation algorithms, emphasising the importance of frequent clear-sky observations. However, there is a dearth of

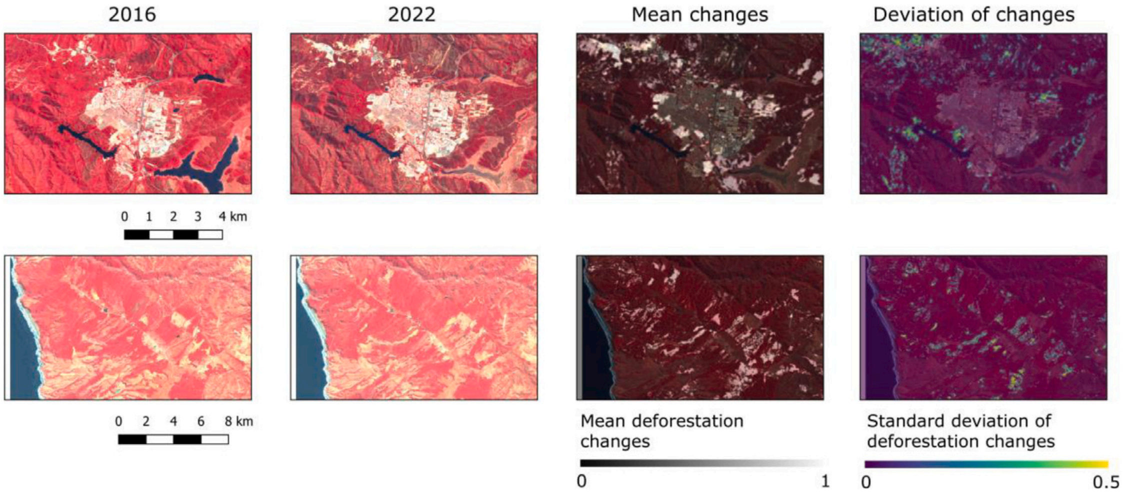

Fig. 9. Deforestation changes tracked. Two zoomed-in regions are depicted with mean false colour (NIR-red-green) images for the years 2016 and 2022. Mean deforestation changes and standard deviation deforestation changes from the 10-fold validation are also shown.

studies investigating the effects of observation frequency on change detection. Lunetta et al. (2004) explored frequencies of 3, 7, and 10 years using Landsat images to track land cover changes, finding that a frequency of at least 3 years is needed to appropriately detect changes in North Carolina, USA. However, further research is needed to transfer these findings to other site conditions and satellites. Harmonising and combining Landsat and Sentinel 2 datasets can potentially increase observation frequency (Claverie et al., 2018), and their effects on change detection should be further examined.

4.2. Disentangling human- and natural-induced forest changes

As discussed previously, optical data solely is often insufficient to determine the nature of the detected changes (Bannari et al., 1995). While NDVI values can serve as a proxy for vegetation presence or greenness (Chapungu et al., 2020), the NDVI values cannot directly provide information about the cause or driver of the disturbances. Therefore, a significant change in the NDVI time series can be caused by varying natural- and human-made drivers (Jackson and Huete, 1991). For instance, we found widespread systematic disturbances throughout central Chile during the summer of 2020, which resulted from browning and prolonged drought conditions (Fig. 8) (Miranda et al., 2020, 2022). The systematic breaks identified during the summer of 2020 were associated with a "browning" process affecting native vegetation. This indicates a systematic decline in vegetation health or vegetation death, which can be observed through changes in NDVI or productivity measures (Koulgi et al., 2019). Other studies have observed a similar phenomenon in other areas of the globe (Hao et al., 2022).

We identified deforestation changes by leveraging spatial and temporal occurrence patterns of the overall unsupervised change detection. We used, in this case, a secondary supervised classification approach as suggested by Cohen et al. (2018) when studying the potential extrapolation of change detection methods, incorporating neighbourhood data and textural analysis of change detections and magnitudes as covariates to disentangle deforestation from other forest disturbances. We also included topographic and radar data to integrate structural changes in the vegetation canopies as additional information aiding the identification of deforestation (Reiche et al., 2018). However, further research is needed to explore the importance of covariates in the deforestation detection.

4.3. Policy-making and management

Overall, we found that in various cases the remotely sensed change detection approach significantly reduced the response time compared to citizen complaints managed by the Environmental Superintendence (Fig. 9). This further highlights the potential for prompt action if automated methodologies like this one are integrated into governance schemes. Depicting change detection at the landscape level is crucial for monitoring unauthorised activities, such as logging and specific urban expansions, reducing the environmental impacts and the expenses associated with *in-situ* monitoring and control by the government. However, it is essential to approach public complaints with caution. While some complaints contain specific information related to deforestation (Table S1, Supplementary materials), they often lack information about the nature, magnitude, or extent of the disturbance. Moreover, the georeferencing of complaints can be inaccurately provided by users, leading to cases of low NDVI values, making categorising the locations as forests or closed shrublands challenging. Therefore, while these complaint datasets can serve as a reference for further investigation and comparison, they should not be considered as real validation sources.

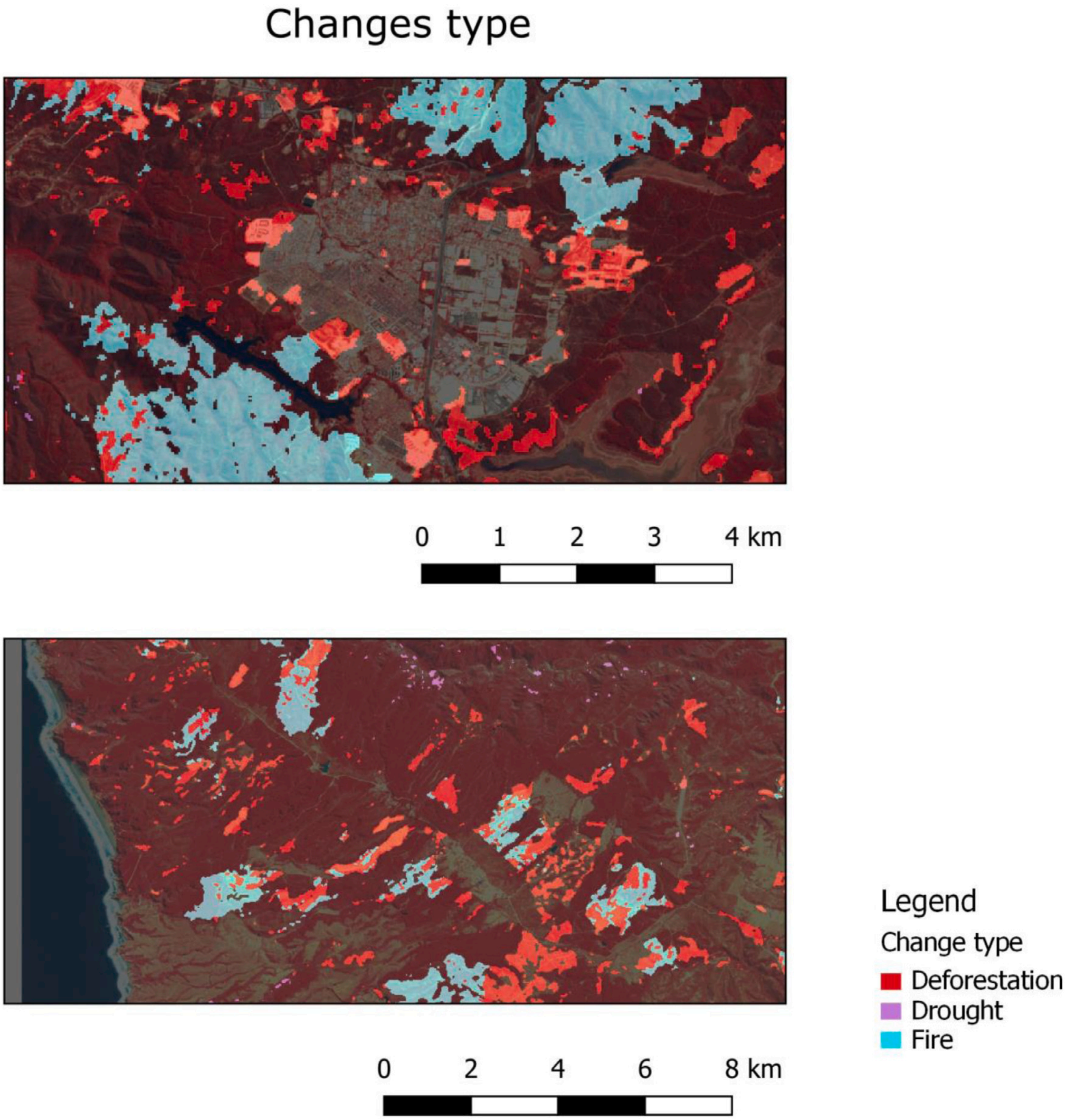

Fig. 10. Deforestation changes tracked. Two zoomed-in regions are depicted with mean false colour (NIR-red-green) images for the years 2016 and 2022. Mean deforestation changes and standard deviation deforestation changes from the 10-fold validation are also shown.

5. Conclusions

Forest ecosystems were monitored using phenological characterisation and temporal segmentation algorithms. While the temporal segmentation through PELT slightly outperformed other methods for deforestation tracking using NDVI calculated from the Landsat dataset, it also led to a high latency between deforestation and its detection. CCDC leads to a generally good performance and a fast deforestation detection response. We observed the general tendencies of the three methods to depict forest decline due to severe drought conditions and large fires. This implies that the separation of these events from human-based interventions is challenging. Disentangling deforestation from other changes through a secondary classification using neighbourhood statistics and textural analysis applied to the detected changes, together with topographic and radar data, led to robust results. Additionally, deforestation detection was assertive when evaluated against citizen complaints raised to the Environmental Superintendence, leading, on average, to a faster detection (94 days before than complaints). Further research is needed to assess other alternatives depicting human-based forest disturbances through, for example, deep learning methods.

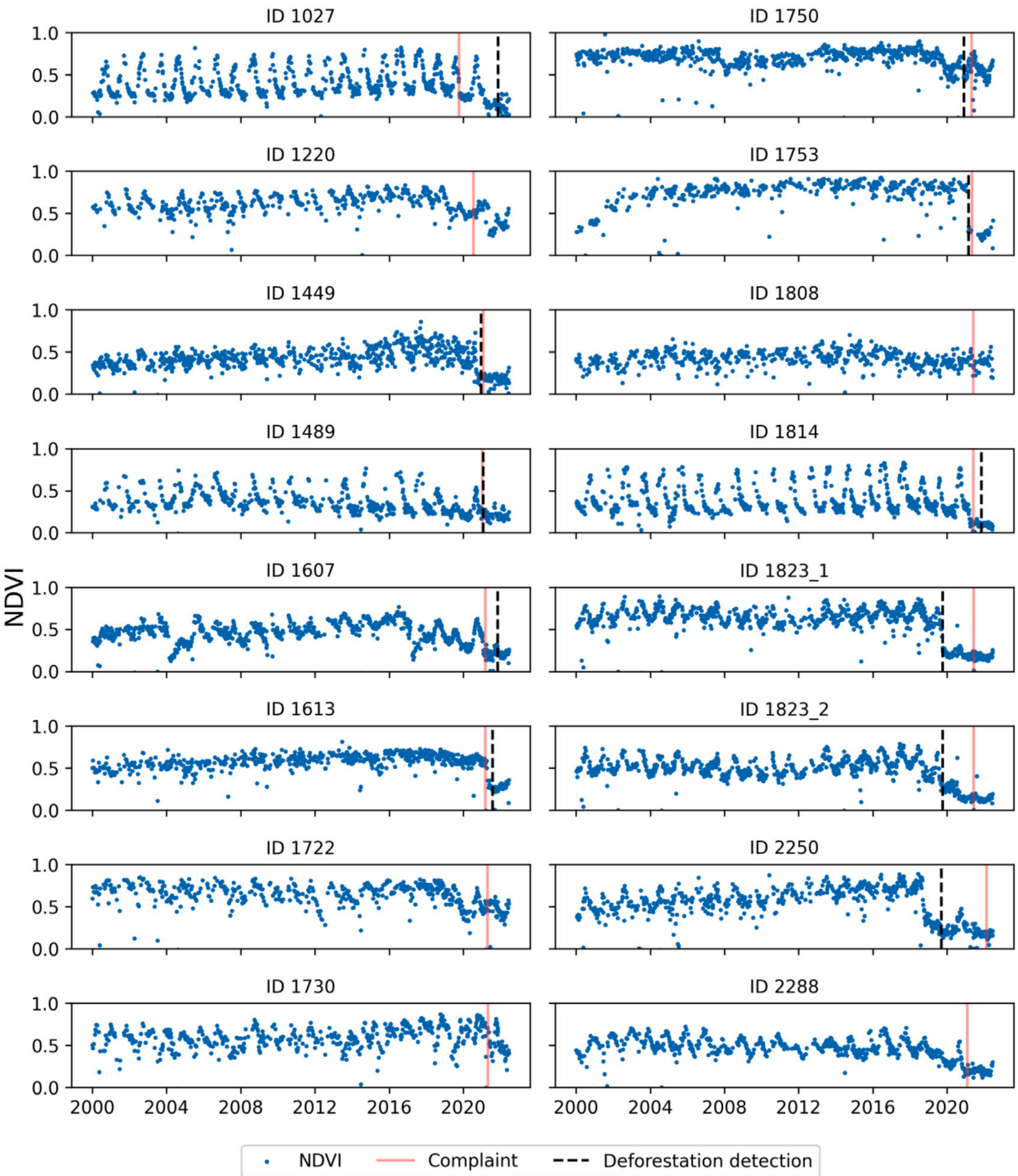

Fig. 11. Different series for locations of citizen-based complaints raised to the Environmental Superintendence and deforestation detection results.

Code availability

The code associated with this project will be made available in the following repository: https://github.com/IFuentesSR/samsara_deforestation

CRediT authorship contribution statement

Ignacio Fuentes: Data curation, Conceptualization, Formal analysis, Investigation, Methodology, Software, Validation, Writing – original draft, Writing – review & editing. **Javier Lopatin:** Conceptualization, Funding acquisition, Methodology, Writing – original draft, Writing – review & editing. **Mauricio Galleguillos:** Conceptualization, Methodology, Project administration, Writing – original draft, Writing – review & editing. **Andrés Ceballos-Comisso:** Conceptualization, Data curation. **Susana Eyheramendy:**

Conceptualization, Funding acquisition, Writing – review & editing. **Rodrigo Carrasco:** Writing – review & editing, Funding acquisition, Conceptualization.

Declaration of competing interest

The authors declare the following financial interests/personal relationships which may be considered as potential competing interests: Ignacio Fuentes reports financial support was provided by National Agency for Research and Development. Mauricio Galleguillos reports financial support was provided by Fund for the Promotion of Scientific and Technological Development.

Data availability

Data used is Publicly available, and data sources were properly referenced.

Acknowledgements

This project was supported by the 'SAMSARA' FONDEF IdeA I+D ID21I10102 project, ANID, Chile. Ignacio is also funded by the ANID FONDECYT Postdoctoral Project N° 3220317.

Appendix A. Supplementary data

Supplementary material related to this article can be found online at https://doi.org/10.1016/j.rsase.2024.101210.

References

Alaniz, A.J., Galleguillos, M., Perez-Quezada, J.F., 2016. Assessment of quality of input data used to classify ecosystems according to the IUCN Red List methodology: The case of the central Chile hotspot. Biol. Cons. 204, 378–385.

Arcanjo, J.S., Luz, E.F., Fazenda, Á.L., Ramos, F.M., 2016. Methods for evaluating volunteers' contributions in a deforestation detection citizen science project. Future Gener. Comput. Syst. 56, 550–557.

Asokan, A., Anitha, J., 2019. Change detection techniques for remote sensing applications: A survey. Earth Sci. Inform. 12 (2), 143–160.

Attiwill, P.M., Adams, M.A., 1993. Nutrient cycling in forests. New Phytol. 124 (4), 561–582.

Bakker, K., Ritts, M., 2018. Smart earth: A meta-review and implications for environmental governance. Glob. Environ. Change 52, 201–211.

Bannari, A., Morin, D., Bonn, F., Huete, A., 1995. A review of vegetation indices. Remote Sens. Rev. 13 (1–2), 95–120.

Baret, F., Hagolle, O., Geiger, B., Bicheron, P., Miras, B., Huc, M., Berthelot, B., Niño, F., Weiss, M., Samain, O., et al., 2007. LAI, FAPAR and fcover CYCLOPES global products derived from vegetation: Part 1: Principles of the algorithm. Remote Sens. Environ. 110 (3), 275–286.

Barlow, J., Lennox, G.D., Ferreira, J., Berenguer, E., Lees, A.C., Nally, R.M., Thomson, J.R., Ferraz, S.F.d., Louzada, J., Oliveira, V.H.F., et al., 2016. Anthropogenic disturbance in tropical forests can double biodiversity loss from deforestation. Nature 535 (7610), 144–147.

Beck, H.E., Zimmermann, N.E., McVicar, T.R., Vergopolan, N., Berg, A., Wood, E.F., 2018. Present and future Köppen-Geiger climate classification maps at 1-km resolution. Sci. Data 5 (1), 1–12.

Bengtsson, J., Nilsson, S.G., Franc, A., Menozzi, P., 2000. Biodiversity, disturbances, ecosystem function and management of European forests. For. Ecol. Manag. 132 (1), 39–50.

Boisier, J.P., Rondanelli, R., Garreaud, R.D., Muñoz, F., 2016. Anthropogenic and natural contributions to the Southeast Pacific precipitation decline and recent megadrought in central Chile. Geophys. Res. Lett. 43 (1), 413–421.

Bottalico, F., Travaglini, D., Chirici, G., Garfì, V., Giannetti, F., De Marco, A., Fares, S., Marchetti, M., Nocentini, S., Paoletti, E.o., 2017. A spatially-explicit method to assess the dry deposition of air pollution by urban forests in the city of florence, Italy. Urban Forest. Urban Green. 27, 221–234.

Cai, Y., Shi, Q., Xu, X., Liu, X., 2023. A novel approach towards continuous monitoring of forest change dynamics in fragmented landscapes using time series Landsat imagery. Int. J. Appl. Earth Obs. Geoinf. 118, 103226.

Canadell, J.G., Meyer, C., Cook, G.D., Dowdy, A., Briggs, P.R., Knauer, J., Pepler, A., Haverd, V., 2021. Multi-decadal increase of forest burned area in Australia is linked to climate change. Nat. Commun. 12 (1), 6921.

Castillo, M., Plaza, Á., Garfias, R., 2020. A recent review of fire behavior and fire effects on native vegetation in Central Chile. Global Ecol. Conserv. 24, e01210.

Chapungu, L., Nhamo, L., Gatti, R.C., 2020. Estimating biomass of savanna grasslands as a proxy of carbon stock using multispectral remote sensing. Remote Sens. Appl.: Soc. Environ. 17, 100275.

Chávez, R.O., Moreira-Muñoz, A., Galleguillos, M., Olea, M., Aguayo, J., Latín, A., Aguilera-Betti, I., Muñoz, A.A., Manríquez, H., 2019. GIMMS NDVI time series reveal the extent, duration, and intensity of "blooming desert" events in the hyper-arid Atacama Desert, Northern Chile. Int. J. Appl. Earth Obs. Geoinf. 76, 193–203.

Chen, S., Wen, Z., Ma, M., Wu, S., 2021. Disentangling climatic factors and human activities in governing the old and new forest productivity. Remote Sens. 13 (18), 3746.

Claverie, M., Ju, J., Masek, J.G., Dungan, J.L., Vermote, E.F., Roger, J.-C., Skakun, S.V., Justice, C., 2018. The harmonized Landsat and sentinel-2 surface reflectance data set. Remote Sens. Environ. 219, 145–161.

Cohen, W.B., Healey, S.P., Yang, Z., Stehman, S.V., Brewer, C.K., Brooks, E.B., Gorelick, N., Huang, C., Hughes, M.J., Kennedy, R.E., et al., 2017. How similar are forest disturbance maps derived from different Landsat time series algorithms? Forests 8 (4), 98.

Cohen, W.B., Yang, Z., Healey, S.P., Kennedy, R.E., Gorelick, N., 2018. A LandTrendr multispectral ensemble for forest disturbance detection. Remote Sens. Environ. 205, 131–140.

Cowling, R.M., Rundel, P.W., Lamont, B.B., Arroyo, M.K., Arianoutsou, M., 1996. Plant diversity in Mediterranean-climate regions. Trends Ecol. Evol. 11 (9), 362–366.

Danielsen, F., Burgess, N.D., Balmford, A., Donald, P.F., Funder, M., Jones, J.P., Alviola, P., Balete, D.S., Blomley, T., Brashares, J., et al., 2009. Local participation in natural resource monitoring: A characterization of approaches. Conserv. Biol. 23 (1), 31–42.

de Oliveira Roque, F., Menezes, J.F., Northfield, T., Ochoa-Quintero, J.M., Campbell, M.J., Laurance, W.F., 2018. Warning signals of biodiversity collapse across gradients of tropical forest loss. Sci. Rep. 8 (1), 1–7.

DeFries, R.S., Rudel, T., Uriarte, M., Hansen, M., 2010. Deforestation driven by urban population growth and agricultural trade in the twenty-first century. Nat. Geosci. 3 (3), 178–181.

Dong, J., Metternicht, G., Hostert, P., Fensholt, R., Chowdhury, R.R., 2019. Remote sensing and geospatial technologies in support of a normative land system science: Status and prospects. Curr. Opin. Environ. Sustain. 38, 44–52.
Donoso, P., Donoso, C., 2007. Forest species and stand types of Chile. In: Cubbage, F.W. (Ed.), Forests and Forestry in the Americas: An Encyclopedia. Society of American Foresters and International Society of Tropical Foresters, (Accessed 04 June 2022).
Estay, S., Chávez, R., 2018. Npphen: An R-package for non-parametric reconstruction of vegetation phenology and anomaly detection using remote sensing. p. 301143, BioRxiv.
FAO, 2022. The State of the World's Forests 2022. Forest Pathways for Green Recovery and Building Inclusive, Resilient and Sustainable Economies. Rome.
Ferrante, L., Fearnside, P.M., 2020. The Amazon's road to deforestation. Science 369 (6504), 634.
Figueroa, E., Pasten, R., 2015. The economic value of forests in supplying local climate regulation. Australian J. Agric. Resour. Econ. 59 (3), 446–457.
Filipponi, F., 2019. Sentinel-1 GRD preprocessing workflow. In: Multidisciplinary Digital Publishing Institute Proceedings, vol. 18, (no. 1), p. 11.
Foga, S., Scaramuzza, P., Guo, S., Zhu, Z., Dilley, Jr., R., Beckmann, T., Schmidt, G., Dwyer, J., Hughes, M., Laue, B., 2017. Cloud detection algorithm comparison and validation for operational Landsat data products. Remote Sens. Environ. 194, 379–390.
Fuentes, I., Fuster, R., Avilés, D., Vervoort, W., 2021. Water scarcity in central Chile: The effect of climate and land cover changes on hydrologic resources. Hydrol. Sci. J. 66 (6), 1028–1044.
Fuentes, I., Padarian, J., Van Ogtrop, F., Vervoort, R.W., 2019. Spatiotemporal evaluation of inundated areas using MODIS imagery at a catchment scale. J. Hydrol. 573, 952–963.
Fuentes, I., Padarian, J., Vervoort, R.W., 2022a. Spatial and temporal global patterns of drought propagation. Front. Environ. Sci. 10, URL: https://www.frontiersin.org/article/10.3389/fenvs.2022.788248.
Fuentes, I., Padarian, J., Vervoort, R.W., 2022b. Towards near real-time national-scale soil water content monitoring using data fusion as a downscaling alternative. J. Hydrol. 609, 127705.
Fuentes, I., Vervoort, R.W., McPhee, J., 2024. Global evapotranspiration models and their performance at different spatial scales: Contrasting a latitudinal gradient against global catchments. J. Hydrol. 628, 130477.
Garreaud, R.D., Boisier, J.P., Rondanelli, R., Montecinos, A., Sepúlveda, H.H., Veloso-Aguila, D., 2020. The central Chile mega drought (2010–2018): A climate dynamics perspective. Int. J. Climatol. 40 (1), 421–439.
Gorelick, N., Hancher, M., Dixon, M., Ilyushchenko, S., Thau, D., Moore, R., 2017. Google earth engine: Planetary-scale geospatial analysis for everyone. Remote Sens. Environ. 202, 18–27.
Griffiths, P., Nendel, C., Pickert, J., Hostert, P., 2020. Towards national-scale characterization of grassland use intensity from integrated sentinel-2 and Landsat time series. Remote Sens. Environ. 238, 111124.
Hamilton, S.E., Friess, D.A., 2018. Global carbon stocks and potential emissions due to mangrove deforestation from 2000 to 2012. Nature Clim. Change 8 (3), 240–244.
Hansen, M.C., Krylov, A., Tyukavina, A., Potapov, P.V., Turubanova, S., Zutta, B., Ifo, S., Margono, B., Stolle, F., Moore, R., 2016. Humid tropical forest disturbance alerts using Landsat data. Environ. Res. Lett. 11 (3), 034008.
Hansen, M.C., Potapov, P.V., Moore, R., Hancher, M., Turubanova, S.A., Tyukavina, A., Thau, D., Stehman, S.V., Goetz, S.J., Loveland, T.R., Kommareddy, A., Egorov, A., Chini, L., Justice, C.O., Townshend, J.R.G., 2013. High-resolution global maps of 21st-century forest cover change. Science 342 (6160), 850–853, URL: https://www.science.org/doi/abs/10.1126/science.1244693.
Hao, H., Chen, Y., Xu, J., Li, Z., Li, Y., Kayumba, P.M., 2022. Water deficit may cause vegetation browning in central Asia. Remote Sens. 14 (11), 2574.
Haralick, R.M., Shanmugam, K., Dinstein, I.H., 1973. Textural features for image classification. IEEE Trans. Syst. Man Cybern. (6), 610–621.
Housman, I.W., Chastain, R.A., Finco, M.V., 2018. An evaluation of forest health insect and disease survey data and satellite-based remote sensing forest change detection methods: Case studies in the United States. Remote Sens. 10 (8), 1184.
Huang, C., Goward, S.N., Masek, J.G., Thomas, N., Zhu, Z., Vogelmann, J.E., 2010. An automated approach for reconstructing recent forest disturbance history using dense Landsat time series stacks. Remote Sens. Environ. 114 (1), 183–198.
Hudak, A.T., Wessman, C.A., 2000. Deforestation in Mwanza District, Malawi, from 1981 to 1992, as determined from Landsat MSS imagery. Appl. Geogr. 20 (2), 155–175.
Jackson, R.D., Huete, A.R., 1991. Interpreting vegetation indices. Prevent. Vet. Med. 11 (3–4), 185–200.
Japitana, M.V., Burce, M.E.C., 2019. A satellite-based remote sensing technique for surface water quality estimation. Eng. Technol. Appl. Sci. Res. 9 (2), 3965–3970.
Karthikeyan, L., Chawla, I., Mishra, A.K., 2020. A review of remote sensing applications in agriculture for food security: Crop growth and yield, irrigation, and crop losses. J. Hydrol. 586, 124905, URL: https://www.sciencedirect.com/science/article/pii/S0022169420303656.
Keenan, R.J., Reams, G.A., Achard, F., de Freitas, J.V., Grainger, A., Lindquist, E., 2015. Dynamics of global forest area: Results from the FAO global forest resources assessment 2015. Forest Ecol. Manag. 352, 9–20.
Kerr, Y.H., Waldteufel, P., Wigneron, J.-P., Martinuzzi, J., Font, J., Berger, M., 2001. Soil moisture retrieval from space: The Soil Moisture and Ocean Salinity (SMOS) mission. IEEE Trans. Geosci. Remote Sens. 39 (8), 1729–1735.
Killick, R., Eckley, I.A., Jonathan, P., Chester, U., 2011. Efficient detection of multiple changepoints within an oceano-graphic time series. In: Proceedings of the 58th World Science Congress of ISI. pp. 4137–4142.
Killick, R., Fearnhead, P., Eckley, I.A., 2012. Optimal detection of changepoints with a linear computational cost. J. Amer. Statist. Assoc. 107 (500), 1590–1598.
Kofinas, G.P., 2009. Adaptive co-management in social-ecological governance. In: Principles of Ecosystem Stewardship. Springer, pp. 77–101.
Koulgi, P.S., Clinton, N., Karanth, K.K., 2019. Extensive vegetation browning and drying in forests of India's Tiger Reserves. Sci. Rep. 9 (1), 1–12.
Lary, D.J., Alavi, A.H., Gandomi, A.H., Walker, A.L., 2016. Machine learning in geosciences and remote sensing. Geosci. Front. 7 (1), 3–10.
Leblois, A., Damette, O., Wolfersberger, J., 2017. What has driven deforestation in developing countries since the 2000s? Evidence from new remote-sensing data. World Dev. 92, 82–102.
Löf, M., Madsen, P., Metslaid, M., Witzell, J., Jacobs, D.F., 2019. Restoring forests: Regeneration and ecosystem function for the future. New Forests 50 (2), 139–151.
Loginova, D., Mann, S., 2022. Measuring stability and structural breaks: Applications in social sciences. J. Econ. Surv..
Longo, M., Saatchi, S., Keller, M., Bowman, K., Ferraz, A., Moorcroft, P.R., Morton, D.C., Bonal, D., Brando, P., Burban, B., et al., 2020. Impacts of degradation on water, energy, and carbon cycling of the Amazon tropical forests. J. Geophys. Res.: Biogeosci. 125 (8), e2020JG005677.
Lopatin, J., 2023. Interannual variability of remotely sensed phenology relates to plant communities. IEEE Geosci. Remote Sens. Lett. 20, 1–5.
Lunetta, R.S., Johnson, D.M., Lyon, J.G., Crotwell, J., 2004. Impacts of imagery temporal frequency on land-cover change detection monitoring. Remote Sens. Environ. 89 (4), 444–454.
Mandal, D., Kumar, V., Ratha, D., Dey, S., Bhattacharya, A., Lopez-Sanchez, J.M., McNairn, H., Rao, Y.S., 2020. Dual polarimetric radar vegetation index for crop growth monitoring using sentinel-1 SAR data. Remote Sens. Environ. 247, 111954.
Mansoor, S., Farooq, I., Kachroo, M.M., Mahmoud, A.E.D., Fawzy, M., Popescu, S.M., Alyemeni, M., Sonne, C., Rinklebe, J., Ahmad, P., 2022. Elevation in wildfire frequencies with respect to the climate change. J. Environ. Manag. 301, 113769.
Manuschevich, D., 2018. A critical assessment of the adaptive capacity of land use change in Chile: A socio-ecological approach. In: Land Use-Assessing the Past, Envisioning the Future. IntechOpen.
Masek, J.G., Hayes, D.J., Hughes, M.J., Healey, S.P., Turner, D.P., 2015. The role of remote sensing in process-scaling studies of managed forest ecosystems. Forest Ecol. Manag. 355, 109–123.

Matskovsky, V., Venegas-González, A., Garreaud, R., Roig, F.A., Gutiérrez, A.G., Muñoz, A.A., Le Quesne, C., Klock, K., Canales, C., 2021. Tree growth decline as a response to projected climate change in the 21st century in Mediterranean mountain forests of Chile. Glob. Planet. Change 198, 103406.
McAllister, E., Payo, A., Novellino, A., Dolphin, T., Medina-Lopez, E., 2022. Multispectral satellite imagery and machine learning for the extraction of shoreline indicators. Coast. Eng. 104102.
Miranda, A., Altamirano, A., Cayuela, L., Lara, A., González, M., 2017. Native forest loss in the Chilean biodiversity hotspot: Revealing the evidence. Reg. Environ. Change 17 (1), 285–297.
Miranda, A., Lara, A., Altamirano, A., Di Bella, C., González, M.E., Camarero, J.J., 2020. Forest browning trends in response to drought in a highly threatened Mediterranean landscape of South America. Ecol. Indic. 115, 106401.
Miranda, A., Ovalle, J., Syphard, A., Berdugo, M., Carrasco, J., Mentler, R., Squeo, F., Delpiano, C., Vargas, S., Miranda, M., Dobbs, C., Gómez-González, S., Lara, A., Garreaud, R.D., 2022. Widespread synchronous decline in a Mediterranean forest driven by accelerated aridity. Research Square.
Montoya-Tangarife, C., De La Barrera, F., Salazar, A., Inostroza, L., 2017. Monitoring the effects of land cover change on the supply of ecosystem services in an urban region: A study of Santiago-Valparaíso, Chile. PLoS One 12 (11), e0188117.
Muthuramu, P., Maheswari, T.U., 2019. Tests for structural breaks in time series analysis: A review of recent development. Shanlax Int. J. Econ. 7 (4), 66–79.
Myers, N., Mittermeier, R.A., Mittermeier, C.G., Da Fonseca, G.A., Kent, J., 2000. Biodiversity hotspots for conservation priorities. Nature 403 (6772), 853–858.
Nadrowski, K., Wirth, C., Scherer-Lorenzen, M., 2010. Is forest diversity driving ecosystem function and service? Curr. Opin. Environ. Sustain. 2 (1–2), 75–79.
Nasirzadehdizaji, R., Balik Sanli, F., Abdikan, S., Cakir, Z., Sekertekin, A., Ustuner, M., 2019. Sensitivity analysis of multi-temporal sentinel-1 SAR parameters to crop height and canopy coverage. Appl. Sci. 9 (4), 655.
Olofsson, P., Foody, G.M., Herold, M., Stehman, S.V., Woodcock, C.E., Wulder, M.A., 2014. Good practices for estimating area and assessing accuracy of land change. Remote Sens. Environ. 148, 42–57.
Pang, Y., Zhang, L., Huang, C., Yu, X., Li, Z., 2013. Automatic deforestation detection using time series Landsat images in a tropical forest of China. In: 2013 IEEE International Geoscience and Remote Sensing Symposium-IGARSS. IEEE, pp. 3872–3875.
Parr, T.W., Sier, A.R., Battarbee, R., Mackay, A., Burgess, J., 2003. Detecting environmental change: science and society—perspectives on long-term research and monitoring in the 21st century. Sci. Total Environ. 310 (1–3), 1–8.
Pasquarella, V.J., Arévalo, P., Bratley, K.H., Bullock, E.L., Gorelick, N., Yang, Z., Kennedy, R.E., 2022. Demystifying LandTrendr and CCDC temporal segmentation. Int. J. Appl. Earth Obs. Geoinf. 110, 102806.
Payn, T., Carnus, J.-M., Freer-Smith, P., Kimberley, M., Kollert, W., Liu, S., Orazio, C., Rodriguez, L., Silva, L.N., Wingfield, M.J., 2015. Changes in planted forests and future global implications. Forest Ecol. Manag. 352, 57–67.
Puhm, M., Deutscher, J., Hirschmugl, M., Wimmer, A., Schmitt, U., Schardt, M., 2020. A near real-time method for forest change detection based on a structural time series model and the Kalman filter. Remote Sens. 12 (19), 3135.
Redlich, S., Zhang, J., Benjamin, C., Dhillon, M.S., Englmeier, J., Ewald, J., Fricke, U., Ganuza, C., Haensel, M., Hovestadt, T., et al., 2022. Disentangling effects of climate and land use on biodiversity and ecosystem services—A multi-scale experimental design. Methods Ecol. Evol. 13 (2), 514–527.
Reiche, J., Hamunyela, E., Verbesselt, J., Hoekman, D., Herold, M., 2018. Improving near-real time deforestation monitoring in tropical dry forests by combining dense sentinel-1 time series with Landsat and ALOS-2 PALSAR-2. Remote Sens. Environ. 204, 147–161.
Ribeiro, M.C., Martensen, A.C., Metzger, J.P., Tabarelli, M., Scarano, F., Fortin, M.-J., 2011. The Brazilian Atlantic Forest: A shrinking biodiversity hotspot. In: Biodiversity Hotspots: Distribution and Protection of Conservation Priority Areas. Springer, pp. 405–434.
Ritchie, H., Roser, M., 2021. Forests and Deforestation. Our World in Data.
Rocha-Santos, L., Mayfield, M.M., Lopes, A.V., Pessoa, M.S., Talora, D.C., Faria, D., Cazetta, E., 2020. The loss of functional diversity: A detrimental influence of landscape-scale deforestation on tree reproductive traits. J. Ecol. 108 (1), 212–223.
Rouse, Jr., J., Haas, R., Schell, J., Deering, D., 1973. Paper a 20. In: Third Earth Resources Technology Satellite-1 Symposium: the Proceedings of a Symposium Held by Goddard Space Flight Center at Washington, DC On, vol. 351, p. 309.
Salas, C., Donoso, P.J., Vargas, R., Arriagada, C.A., Pedraza, R., Soto, D.P., 2016. The forest sector in Chile: An overview and current challenges. J. Forest. 114 (5), 562–571.
Sánchez, J.J., Marcos-Martinez, R., Srivastava, L., Soonsawad, N., 2021. Valuing the impacts of forest disturbances on ecosystem services: An examination of recreation and climate regulation services in US national forests. Trees Forests People 5, 100123.
Sarricolea, P., Herrera-Ossandon, M., Meseguer-Ruiz, Ó., 2017. Climatic regionalisation of continental Chile. J. Maps 13 (2), 66–73.
Schultz, M., Clevers, J.G., Carter, S., Verbesselt, J., Avitabile, V., Quang, H.V., Herold, M., 2016. Performance of vegetation indices from Landsat time series in deforestation monitoring. Int. J. Appl. Earth Observ. Geoinform. 52, 318–327.
Schultz, M., Verbesselt, J., Avitabile, V., Souza, C., Herold, M., 2015. Error sources in deforestation detection using BFAST monitor on Landsat time series across three tropical sites. IEEE J. Sel. Top. Appl. Earth Obs. Remote Sens. 9 (8), 3667–3679.
Sebald, J., Senf, C., Seidl, R., 2021. Human or natural? Landscape context improves the attribution of forest disturbances mapped from Landsat in Central Europe. Remote Sens. Environ. 262, 112502.
Silva Junior, C.H., Pessôa, A.C., Carvalho, N.S., Reis, J.B., Anderson, L.O., Aragão, L.E., 2021. The Brazilian Amazon deforestation rate in 2020 is the greatest of the decade. Nat. Ecol. Evol. 5 (2), 144–145.
Smith-Ramírez, C., Castillo-Mandujano, J., Becerra, P., Sandoval, N., Fuentes, R., Allende, R., Acuña, M.P., 2022. Combining remote sensing and field data to assess recovery of the Chilean Mediterranean vegetation after fire: Effect of time elapsed and burn severity. Forest Ecol. Manag. 503, 119800.
Song, C., Lee, W.-K., Choi, H.-A., Kim, J., Jeon, S.W., Kim, J.S., 2016. Spatial assessment of ecosystem functions and services for air purification of forests in South Korea. Environ. Sci. Policy 63, 27–34.
Thakur, S., Mondal, I., Ghosh, P., Das, P., De, T., 2020. A review of the application of multispectral remote sensing in the study of mangrove ecosystems with special emphasis on image processing techniques. Spatial Inform. Res. 28 (1), 39–51.
Truong, C., Oudre, L., Vayatis, N., 2020. Selective review of offline change point detection methods. Signal Process. 167, 107299.
USGS, 2022. Landsat 8-9 Collection 2 (C2), Level 2 Science Product (L2SP) Guide. United States Geological Survey, South Dakota, United States.
Verbesselt, J., Zeileis, A., Herold, M., 2011. Near real-time disturbance detection in terrestrial ecosystems using satellite image time series: Drought detection in Somalia. p. 18, Working Papers in Economics and Statistics.
Wambui, G.D., Waititu, G.A., Wanjoya, A., 2015. The power of the Pruned Exact Linear Time (PELT) test in multiple changepoint detection. Am. J. Theor. Appl. Stat 4 (6), 581–586.
Wand, M.P., Jones, M.C., 1994. Kernel Smoothing. CRC Press.
Weiss, M., Jacob, F., Duveiller, G., 2020. Remote sensing for agricultural applications: A meta-review. Remote Sens. Environ. 236, 111402.
Wu, L., Li, Z., Liu, X., Zhu, L., Tang, Y., Zhang, B., Xu, B., Liu, M., Meng, Y., Liu, B., 2020. Multi-type forest change detection using BFAST and monthly Landsat time series for monitoring spatiotemporal dynamics of forests in subtropical wetland. Remote Sens. 12 (2), 341.
Yin, J., Bauerle, T.L., 2017. A global analysis of plant recovery performance from water stress. Oikos 126 (10), 1377–1388.
Yin, H., Prishchepov, A.V., Kuemmerle, T., Bleyhl, B., Buchner, J., Radeloff, V.C., 2018. Mapping agricultural land abandonment from spatial and temporal segmentation of Landsat time series. Remote Sens. Environ. 210, 12–24.
Zemp, D., Schleussner, C.-F., Barbosa, H.d.J., Rammig, A., 2017. Deforestation effects on Amazon forest resilience. Geophys. Res. Lett. 44 (12), 6182–6190.
Zeng, L., Wardlow, B., Xiang, D., Hu, S., Li, D., 2020. A review of vegetation phenological metrics extraction using time-series, multispectral satellite data. Remote Sens. Environ. 237, 111511.

Zhao, Y., Feng, D., Yu, L., Wang, X., Chen, Y., Bai, Y., Hernández, H.J., Galleguillos, M., Estades, C., Biging, G.S., Radke, J.D., Gong, P., 2016. Detailed dynamic land cover mapping of Chile: Accuracy improvement by integrating multi-temporal data. Remote Sens. Environ. 183, 170–185.

Zhu, Z., 2017. Change detection using Landsat time series: A review of frequencies, preprocessing, algorithms, and applications. ISPRS J. Photogramm. Remote Sens. 130, 370–384.

Zhu, Z., Woodcock, C.E., 2014. Continuous change detection and classification of land cover using all available Landsat data. Remote Sens. Environ. 144, 152–171.